Classical and quantum distinctions between weak and strong coupling

Said Rahimzadeh-Kalaleh Rodriguez[*]

Center for Nanophotonics, FOM Institute AMOLF, c/o Philips Research Laboratories,
High Tech Campus 4, 5656 AE Eindhoven, The Netherlands[†]

(Dated: December 4, 2015)

Coupled systems subject to dissipation exhibit two different regimes known as weak coupling and strong coupling. Two damped coupled harmonic oscillators (CHOs) constitute a model system where the key features of weak and strong coupling can be identified. Several of these features are common to classical and quantum systems, as a number of quantum-classical correspondences have shown. However, the condition defining the boundary between weak and strong coupling is distinct in classical and quantum formalisms. Here we describe the origin of two widely used definitions of strong coupling. Using a classical CHO model, we show that energy exchange cycles and avoided resonance crossings signal the onset of strong coupling according to one criterion. From the classical CHO model we derive a non-Hermitian Hamiltonian describing open quantum systems. Based on the analytic properties of the Hamiltonian, we identify the boundary between weak and strong coupling with a different feature: a non-Hermitian degeneracy known as the exceptional point. For certain parameter ranges the classical and quantum criterion for strong coupling coincide; for other ranges they do not. Examples of systems in strong coupling according to one or another criterion, but not both, are illustrated. The framework here presented is suitable for introducing graduate or advanced undergraduate students to the basic properties of strongly coupled systems, as well as to the similarities and subtle differences between classical and quantum descriptions of coupled dissipative systems.

I. INTRODUCTION

Studies of energy transfer are at the foundation of physics. Two damped coupled harmonic oscillators (CHOs) constitute an illustrative system where the interplay between energy exchange and dissipation can be recognized. The CHOs exchange energy between them via a coupling spring, while they each loose energy to their surroundings via friction. Consequently, qualitatively distinct behavior emerges when one of these processes dominates. In this light, one of the most important distinctions in the physics of coupled dissipative systems is made: weak versus strong coupling. For two CHOs, weak and strong coupling are commonly identified in three contexts: i) the dynamics is governed by exponential decay or energy exchange cycles; ii) the steady-state spectrum of the driven system displays a single resonance or two split peaks; iii) the eigenfrequencies of the CHOs cross or anti-cross as the frequency difference between the bare oscillators transits through zero. Naturally, the analysis of dynamics, steady-state spectra, and eigenvalues also constitute the main arena of the dissipative two-state quantum model.[1] Despite the many parallels between classical and quantum descriptions of coupled dissipative systems[2], two distinct criteria for strong coupling are widespread.

One criterion for strong coupling relies on the energy exchange rate exceeding all loss rates. Novotny quotes a tighter variant of this criterion: 'to observe strong coupling, the frequency splitting [∝ coupling strength] needs to be larger than the sum of the linewidths [∝ loss rates]'.[3] The spectrum of a driven CHO system under this condition displays two split resonances provided that the driving force does not excite only one eigenmode of the system. Hence, in a similar spirit Törmä and Barnes defined the coupling regime based on whether two split peaks are visible in the spectrum (strong coupling) or not (weak coupling).[4]

A second (different) criterion for strong coupling involves the energy exchange rate exceeding the difference between the loss rates rather than their individual magnitudes or their sum (see e.g. Andreani[5] or Laussy *et al.*[6]). This second criterion implies that two identical oscillators with arbitrarily high losses are strongly coupled for any non-zero energy exchange rate. If the energy exchange rate is much less than the loss rates, the strongly coupled system is incapable of exhibiting energy exchange cycles or split peaks in the spectrum. Nevertheless, two levels anti-cross provided that the difference between their loss rates is sufficiently small compared to their energy exchange rate.

The two criteria described above give the same result for many systems deep into the strong or weak coupling regimes. However, intermediate regimes exist where a given system can fulfill one condition for strong coupling but not the other. While the first (second) condition for strong coupling is more often encountered in classical (quantum) formalisms, no particular axiom of classical or quantum mechanics holds any of these criteria above the other. As we will see, it is simply the analysis of different features which gives rise to distinct criteria. Understanding these differences is crucial for assessing the characteristic time scales of a system. This understanding is also relevant in the context of many quantum-classical correspondences, where CHOs have played a prominent role.[3,7–21] Another motivation for distinguishing between weak and strong coupling of CHOs is related to the interpretation of experiments: CHOs are widely used to analyze experimental data based on a best-fit approach
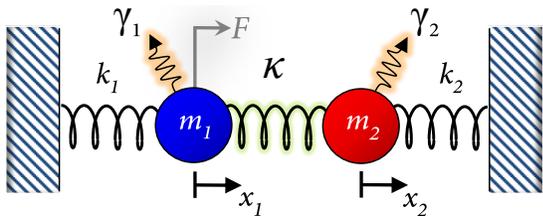
FIG. 1. Two coupled harmonic oscillators. $\gamma_{1,2}$ are the loss rates, $\sqrt{k_{1,2}/m_{1,2}}$ are the eigenfrequencies of the bare oscillators, κ is the coupling spring constant, $x_{1,2}$ are the displacements from equilibrium, and F is a driving force (see text).

(see for example Refs. 22–28 for a far-from exhaustive list). A distinction between weak and strong coupling is necessary to determine whether the constituents of the coupled system merely perturb each other, or their mutual influence is so strong that their individuality is lost.

Here we demonstrate the different features defining the boundary between weak and strong coupling in classical and quantum frameworks. We study the classical CHO dynamics in section II and the steady-state spectra in section III. Therein, we find a transition from weak to strong coupling evidenced by the onset of energy exchange cycles and frequency splitting between the CHOs. In section IV we map the classical CHO model to the two-state non-Hermitian Hamiltonian (NHH) describing open quantum systems. The NHH has a complex energy spectrum, the imaginary part of which represents the losses. The discussion is suitable for introducing students to the non-Hermitian quantum framework. This is becoming increasingly relevant since NHHs have proven to model several physical systems more faithfully than their Hermitian counterparts.[29–34] Amongst the most remarkable features of NHHs lies a non-Hermitian degeneracy known as the exceptional point (EP).[29,32] In section IV we explain the origin of the EP and its relation to the second distinction between weak and strong coupling. More generally, the derivation of a two-state NHH from the equations of motion of two damped CHOs constitutes an insightful exercise whereby students can recognize links between first-order perturbation theory and the intuitive physics of coupled oscillators. In this way, two key elements of the physics curriculum encountered in introductory quantum and classical mechanics courses can be presented in a unified framework. Consequently, students will be able to appreciate a wide range of seemingly abstract quantum phenomena from the classical perspective of coupled oscillators, while requiring only a basic knowledge of linear algebra, ordinary differential equations, and complex analysis.

II. DYNAMICS OF COUPLED HARMONIC OSCILLATORS

We first study the dynamics of two damped CHOs as illustrated in Fig. 1. In the absence of any driving force

($F = 0$), the equations of motion are,

$$\ddot{x}_1 + \gamma_1 \dot{x}_1 + \omega_1^2 x_1 - \Omega^2 x_2 = 0,$$
$$\ddot{x}_2 + \gamma_2 \dot{x}_2 + \omega_2^2 x_2 - \Omega^2 x_1 = 0. \quad (1)$$

x_j ($j = 1, 2$) is the displacement from equilibrium of the jth oscillator, which has an uncoupled eigenfrequency $\omega_j = \sqrt{k_j/m_j}$ and a loss rate γ_j. Let us first consider two identical oscillators: $m_1 = m_2 = m$, $k_1 = k_2 = k$, $\omega_1 = \omega_2 = \omega_0$ and $\gamma_1 = \gamma_2 = \gamma$. The oscillators are coupled at a rate $\Omega = \sqrt{\kappa/m}$, where κ is the stiffness constant of the middle spring. We focus on underdamped oscillators ($\gamma/2 < \omega_0$) which are best suited for distinguishing between weak and strong coupling. We refer to Ref. 35 for the overdamped ($\gamma/2 > \omega_0$) case and the corresponding quantum-classical correspondence.

We are interested in the time-evolution of the total energy in the oscillators when one of the oscillators is initially displaced from equilibrium, i.e., $x_1(0) \neq 0$ and $x_2 = 0$. We can solve this problem numerically in matrix form using the state-space representation. For this purpose, the two second order differential equations (Eq. 1) are reduced to four first order differential equations. The state variables representing the system are

$$q_1 = x_1,$$
$$q_2 = \dot{x}_1,$$
$$q_3 = x_2,$$
$$q_4 = \dot{x}_2. \quad (2)$$

These variables form the state vector $\mathbf{q}$, whose time-evolution obeys the following matrix differential equation:

$$\begin{bmatrix} \dot{q}_1 \\ \dot{q}_2 \\ \dot{q}_3 \\ \dot{q}_4 \end{bmatrix} = \begin{bmatrix} 0 & 1 & 0 & 0 \\ -\omega_1^2 & -\gamma_1 & \Omega^2 & 0 \\ 0 & 0 & 0 & 1 \\ \Omega^2 & 0 & -\omega_2^2 & -\gamma_2 \end{bmatrix} \begin{bmatrix} q_1 \\ q_2 \\ q_3 \\ q_4 \end{bmatrix}. \quad (3)$$

We solve Eq. 3 numerically, setting $\omega_0 = 1$ rad/s and $\gamma = 10^{-3}\omega_0$. We calculate the total energy in oscillators 1 and 2 given by the sum of the kinetic and potential energies, $T_{1,2}$ and $V_{1,2}$, respectively. In terms of the state variables, $T_1 + V_1 = \frac{mq_2^2}{2} + \frac{kq_1^2}{2}$ and $T_2 + V_2 = \frac{mq_4^2}{2} + \frac{kq_3^2}{2}$.

In Fig. 2 we plot $T_{1,2} + V_{1,2}$ as a function of the dimensionless time constant $\Omega^2 t/(2\pi\omega_0)$ for three values of the ratio $\Omega^2/\omega_0\gamma$. When $\Omega^2 < \omega_0\gamma$, loss dominates over energy exchange. An example is shown in Fig. 2(a), where $\Omega^2/\omega_0\gamma = 0.5$. The initial energy stored in oscillator 1 (blue line) is dissipated before it can be transferred to oscillator 2 (red line). The dynamics is qualitatively similar for $\Omega = 0$ (not shown), where the total energy in oscillator 1 decays as $e^{-2\gamma t}$ (black dotted line). Hence, the weak coupling simply exerts a perturbative effect on the exponential energy decay of the excited CHO.

A different regime arises when $\Omega^2 > \omega_0\gamma$. We plot the dynamics for $\Omega^2/\omega_0\gamma = 1.1$ in Fig. 2(c), and for
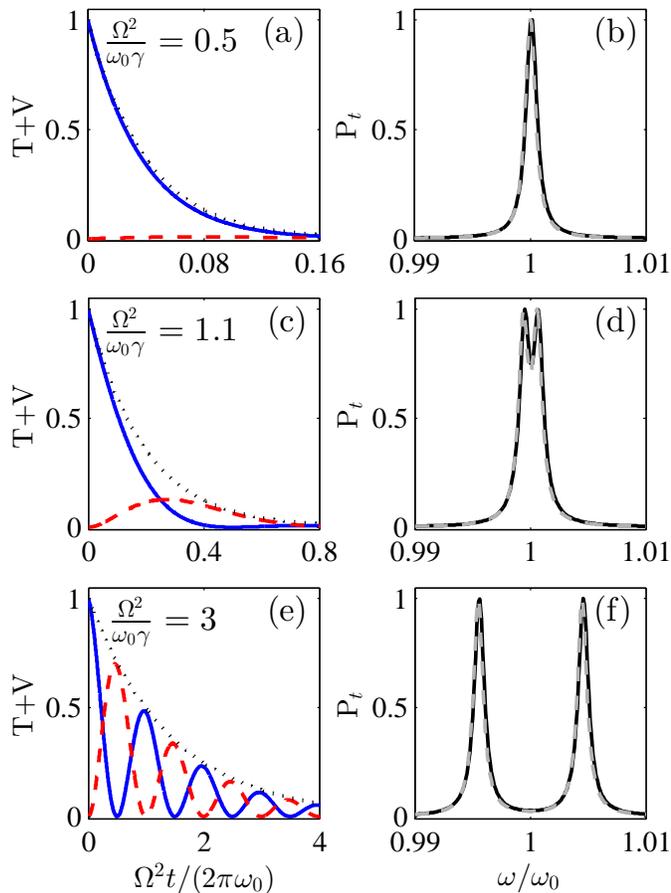
FIG. 2. (a,c,e) show the time evolution of the total energy (kinetic T plus potential V) in two coupled harmonic oscillators. Ω is the coupling rate, γ is the loss rate, and ω_0 is the eigenfrequency of the bare oscillators. The blue solid line is the energy in oscillator 1, the red dashed line is the energy in oscillator 2, and the dotted black line is $e^{-2\gamma t}$. In (b, d, f) the black solid line is the time-integrated dissipated power by both oscillators. The overlying grey dashed line is the steady-state dissipated power by both oscillators when only one oscillator is driven by a time-harmonic force.

$\Omega^2/\omega_0\gamma = 3$ in Fig. 2(e). In Fig. 2(c) we observe a single cycle of energy exchange between the CHOs, while in Fig. 2(e) we observe multiple cycles. The observation of energy exchange cycles indicates that the CHOs transfer energy between them faster than they each dissipate energy. The observation of this effect is therefore often associated with the strong coupling regime. It is noteworthy that, within the classical formalism, observing energy exchange cycles requires initially displacing one of the oscillators from its equilibrium position. This means that energy needs to be externally fed into the system. According to quantum theory, this needs not be the case; an atom in a cavity can exchange energy with the vacuum field.[36]

Figure 2 sheds light on a smooth boundary between weak and strong coupling at $\Omega^2/\omega_0\gamma \approx 1$. Note that for
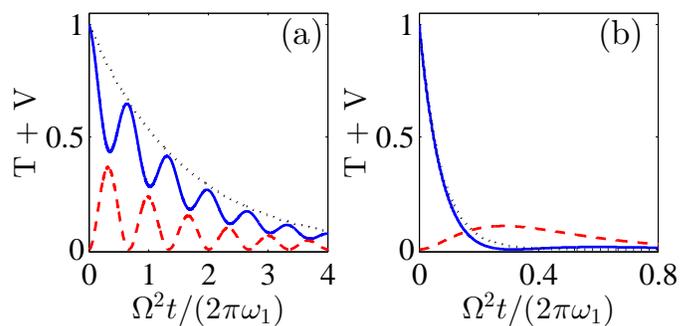

FIG. 3. Time evolution of the total energy in two coupled harmonic oscillators with unequal eigenfrequencies in (a) and unequal loss rates in (b). For both plots $\omega_1 = 1$ rad/s and $\Omega_1 = 0.1$ rad/m. In (a): $\omega_2 = 0.989$ rad/s and $\gamma_1 = \gamma_2 = 1$ mrad/s. In (b) $\omega_2 = \omega_1$, $\gamma_1 = 22$ mrad/s and $\gamma_2 = 1$ mrad/s.

$\gamma_1 = \gamma_2 = \gamma$ we have $\Omega^2/\omega_0\gamma = 2\Omega^2/\omega(\gamma_1 + \gamma_2)$. Hence, the above definition of strong coupling is sometimes expressed in terms of the sum of the loss rates.[3] While the sum of the loss rates is a decisive factor for observing energy exchange cycles, the difference between the loss rates is not. Consider that $|\gamma_1 - \gamma_2| = 0$ for all three cases in Fig. 2, yet a significantly different amount of energy exchange is observed for each case. Thus, qualitatively distinct behavior emerges even though the difference between the loss rates remains unchanged. In section IV we will discuss the relevance of the quantity $|\gamma_1 - \gamma_2|$. By analyzing different features, we will show that the value of $|\gamma_1 - \gamma_2|$ compared to the value of Ω can serve to define the boundary between two distinct regimes also known as weak coupling and strong coupling.

Next we analyze the time-integrated power spectrum of the undriven initially excited CHOs. The frequency-dependence of the jth oscillator's displacement from equilibrium is obtained by Fourier-transforming its time-dependent displacement from equilibrium, viz.,

$$X_j(\omega) = \frac{1}{\sqrt{2\pi}} \int_{-\infty}^{\infty} x_j(t)e^{-i\omega t}dt. \qquad (4)$$

The time-integrated dissipated power spectrum is given by

$$P_j(\omega) = \omega_j^2 \gamma_j |X_j(\omega)|^2. \qquad (5)$$

In Figs. 2(b, d, f) we show as black solid lines the total absorbed power spectrum $P_t = P_1 + P_2$ for the corresponding time-traces in Figs. 2(a, c, e). We normalize each spectrum because we are interested in qualitative behavior only. The spectra show the frequency splitting of a single resonance into two resonances as the coupling strength increases. This effect is often referred to as "Rabi splitting" or "Autler-Townes splitting", and it is regarded as the spectral signature of the transition to strong coupling. The split peaks are centered at the eigenfrequency of the bare (identical) oscillators.

In addition to the condition $\Omega^2/\omega_0\gamma \gtrsim 1$, observing energy exchange cycles requires that the initial conditions do not match an eigenmode of the system. The CHO eigenmodes involve the combined harmonic motion of the two oscillators in phase (symmetric mode) or π-dephased (anti-symmetric mode). These modes are excited for the initial conditions $x_1(0) = x_2(0) \neq 0$ and $x_1(0) = -x_2(0) \neq 0$, respectively. If an eigenmode is directly excited, the strong coupling dynamics is governed by exponential energy decay, as in weak coupling. The corresponding power spectrum displays a single resonance peak shifted from ω_0 by an amount proportional to Ω. The shift is to lower frequencies when the symmetric mode is excited, and to higher frequencies when the anti-symmetric mode is excited.

Notice in Fig. 2(e) that the CHOs undergo complete energy exchange at integer multiples of the time constant $\Omega^2 t/(2\pi\omega_0)$. This changes when the oscillators are detuned, as we now show. We consider the dynamics of CHOs with unequal eigenfrequencies in Fig. 3(a), and with unequal loss rates in Fig. 3(b). The rates used in the calculations are reported in the figure caption; their choice will be clarified below. Figure 3(a) shows that energy exchange cycles persist despite the detuning $\omega_1 - \omega_2 = 11$ mrad/s. In other words, the oscillators undergo exchange energy cycles even though their eigenfrequencies are significantly different. However, in contrast to the zero-detuning case where $\omega_1 = \omega_2$ [e.g. Fig. 2(e)], the initially excited oscillator stores more energy than its coupled partner at all times. For much greater detunings energy exchange cycles vanish and the dynamics resembles that of weak coupling instead. Figure 3(b) displays roughly a single cycle of energy exchange between CHOs with $(\gamma_1 - \gamma_2)/2 = 11.5$ mrad/s. The behavior in this case is similar to that in Fig. 2(b), where the oscillators had equal loss rates and they were just above the onset of strong coupling. Notice in particular that oscillator 2 (red line) receives a significant fraction of the energy from oscillator 1 (blue line), which contrasts with the weak coupling scenario depicted in Fig. 2(a). Thus, the oscillators undergo significant energy exchange even though their loss rates are rather different.

In preparation for section IV, let us evaluate for all systems in Fig. 2 and Fig. 3 the dimensionless quantity $\Omega^2/\omega_m\Delta$, whose relevance will be clarified further ahead. $\Delta = (\omega_1 - \omega_2) - i(\gamma_1 - \gamma_2)/2$ is the complex detuning of the bare oscillators and $\omega_m = (\omega_1 + \omega_2)/2$ is their mean eigenfrequency. Since $\Delta = 0$ for all systems in Fig. 2, $\Omega^2/\omega_m\Delta = \infty$. Therefore, the quantity $\Omega^2/\omega_m\Delta$ does not in general distinguish between systems that exchange energy efficiently [e.g. Fig. 2(e)] and those that do not [e.g. Fig. 2(a)]. Conversely, Figs. 3(a,b) illustrate two systems for which $\Omega^2/\omega_m\Delta < 1$ yet significant energy exchange cycles are visible. In particular, for the calculation in Figs. 3(a) we set $\Omega^2/\omega_m\Delta = \Omega^2/\omega_m(\omega_1 - \omega_2) = 0.91$, while for Fig. 3(b) we set $\Omega^2/\omega_m\Delta = 2\Omega^2/\omega_m(\gamma_1 - \gamma_2) = 0.95$. The significance of these cases will be discussed in section IV, where we derive a different condition for strong coupling based on $\Omega^2/\omega_m\Delta \geq 1$.

III. DRIVEN-DISSIPATIVE COUPLED HARMONIC OSCILLATORS

In this section we analytically calculate the steady-state power dissipated by a driven system of CHOs. We first consider the excitation of oscillator 1 only. The oscillator is driven by a harmonic force of amplitude per unit mass F and frequency ω. Thus, we add the term $Fe^{-i\omega t}$ to the right hand side of the top Eq. 1. Inserting the ansatz $x_j(t) = x_j^0 e^{-i\omega t}$ in Eq. 1, we obtain the following matrix equations describing the driven-dissipative CHOs:

$$\begin{bmatrix} \omega_1^2 - \omega^2 - i\gamma_1\omega & -\Omega^2 \\ -\Omega^2 & \omega_2^2 - \omega^2 - i\gamma_2\omega \end{bmatrix} \begin{bmatrix} x_1 \\ x_2 \end{bmatrix} = \begin{bmatrix} Fe^{-i\omega t} \\ 0 \end{bmatrix}. \tag{6}$$

Equation 6 has the form $\mathbf{Zx} = \mathbf{F}$. Rearranging as $\mathbf{x} = \mathbf{Z}^{-1}\mathbf{F}$ leads to

$$\begin{bmatrix} x_1 \\ x_2 \end{bmatrix} = \frac{1}{|\mathbf{Z}|} \begin{bmatrix} \omega_2^2 - \omega^2 - i\gamma_2\omega & \Omega^2 \\ \Omega^2 & \omega_1^2 - \omega^2 - i\gamma_1\omega \end{bmatrix} \begin{bmatrix} Fe^{-i\omega t} \\ 0 \end{bmatrix}, \tag{7}$$

with $|\mathbf{Z}| = (\omega_1^2 - \omega^2 - i\omega\gamma_1)(\omega_2^2 - \omega^2 - i\omega\gamma_2) - \Omega^4$. In steady-state, the power dissipated by the jth oscillator at the driving frequency ω is $P_j = \omega^2\gamma_j|x_j(\omega)|^2$.

In Figs. 2(b, d, f) we plot as grey dashed lines the total steady-state dissipated power spectrum $P_t = P_1 + P_2$ calculated for the same model parameters used to calculate the dynamics in Figs. 2(a, c, e). We find an excellent agreement between the steady-state and the time-integrated dynamical response (black lines) of the system. The criterion for strong coupling is therefore identical.

Now we examine a feature commonly associated with strong coupling: avoided resonance crossing (ARC). An ARC arises when two resonances approach, and then repel, each other in frequency as some parameter is varied. For driven CHOs, this parameter can be the uncoupled eigenfrequency detuning $\delta = \omega_2 - \omega_1$. We illustrate the ARC phenomenon in Fig. 4 by calculating the dissipated power P_t as a function of the driving frequency ω and of the detuning parameter δ. The driven frequency is referenced to $\omega_0 = \omega_1$ for convenience. The losses of both oscillators are constant: $\gamma = 10^{-3}\omega_0$. Figure 4(a) shows results for $\Omega^2/\omega_0\gamma = 1$, and Figure 4(b) corresponds to $\Omega^2/\omega_0\gamma = 2$. The two resonances that anti-cross near zero detuning ($\delta = 0$) constitute the ARC, and their splitting at $\delta = 0$ is the so-called Rabi splitting. In Fig. 4(a) we observe that for $|\delta/\gamma| \gtrsim 1$ the spectrum is dominated by a single resonance depending only weakly on δ. This is essentially the driven oscillator resonance. Since the CHOs are at the aforementioned smooth boundary between weak and strong coupling, a
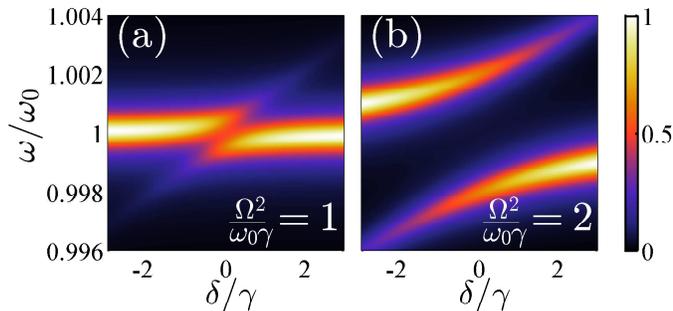
FIG. 4. Total power absorbed in steady-state by two coupled harmonic oscillators with variable frequency detuning δ for two different values of $\Omega^2/\omega_0\gamma$ (see insets). In both plots, only the first oscillator with fixed eigenfrequency ω_0 is driven by a harmonic force with frequency ω.
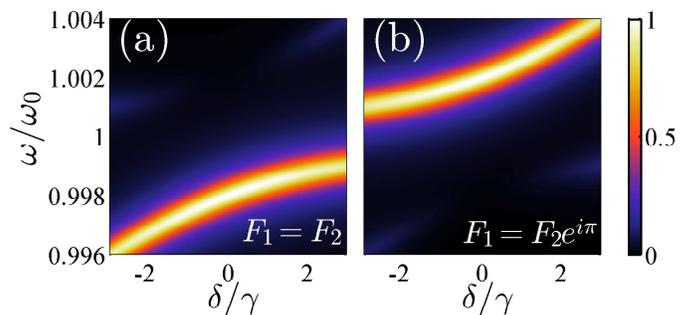

FIG. 5. Total power absorbed in steady-state by two coupled harmonic oscillators with $\Omega^2/\omega\gamma = 2$ and for variable frequency detuning δ. For both plots the oscillators are each driven by a time-harmonic force with equal frequency ω and amplitude per unit mass F. In (a) the two driving forces have equal phase ($F_1 = F_2$), while in (b) they are π-dephased ($F_1 = -F_2$).

detuning of one linewidth is sufficient to practically vanish the influence of the second oscillator on the driven one. This changes for a stronger coupling strength as in Fig. 4(b). Notice in Fig. 4(b) that two resonances well separated in frequency seem to approach, but then repel, each other as δ passes through zero; this is a clear ARC. The resonances in Fig. 4(b) also deviate more from the uncoupled oscillator eigenfrequencies for a given δ than their counterparts in Fig. 4(a); this is expected due to the stronger coupling strength in Fig. 4(b).

ARC is a sufficient but not a necessary signature of strong coupling. The CHO response depends on the match between the driving force and the eigenmodes of the system. When only one oscillator is directly driven, ARCs are observed because both the symmetric and antisymmetric modes can be excited with equal strength. This is no longer the case when both oscillators are directly driven and their relative phase is thereby imposed by the driving force. For example, consider the case where the two forces have equal amplitude and frequency. Thus, $Fe^{i\omega t+\phi}$ is included in the second row of the rightmost term in equations 6 and 7. We present the case $\phi = 0$ in Fig. 5(a), and $\phi = \pi$ in Fig. 5(b). The lower branch is excited much more strongly in Fig. 5(a), while the opposite is true in Fig. 5(b). At $\delta = 0$ each driving scheme excites one resonance only, corresponding to the symmetric mode in Fig. 5(a) and to the anti-symmetric mode in Fig. 5(b). For $\delta \neq 0$ each oscillator supports symmetric and anti-symmetric modes at slightly different frequencies. Consequently, the net driving force no longer matches any one of the eigenmodes perfectly. Notice that the upper resonance branch is progressively, although weakly, excited as $|\delta|$ increases Fig. 5(a). A similar effect occurs for the lower resonance branch in Fig. 5(b).

Our spectral analysis has focused on a single observable — the total dissipated power. However, several experiments have been interpreted through a fit of the dissipated power by one oscillator only,[10,11,37] or the CHO eigenvalues.[26,28] A clear-cut distinction between

weak and strong coupling is more difficult in such cases. The response of the two oscillators can in fact be pronouncedly different near the boundary between weak and strong coupling.[37] Studies of strong light-matter coupling have shown that the observable frequency splitting depends on how the system is probed, e.g. transmission, reflection, or absorption.[38,39] The emission spectrum can also display a different frequency splitting.[27] Therefore, relating an observable in experiments with its counterpart in a fitted CHO model requires careful consideration. In this sense, the total dissipated power by the experimental and CHO model systems seem like a good figure of merit to demonstrate energy transfer between oscillators. While it may not always be easy to experimentally measure it, analyzing the total dissipated power will likely lead to a more faithful mapping of the coupling regime of a system. Ref. 27 illustrates a similar approach for a nanophotonic system. Ref. 39 presents an interesting molecule-cavity system which can be actively tuned in and out of the strong coupling regime; all relevant observables (including the dissipated power) were obtained therein. Finally, Ref. 25 illustrates an interesting alternative approach. The authors of Ref. 25 deduce the coupling and loss rates of a molecule-nanoparticle system by analyzing its scattering spectrum with a CHO model.

IV. NON-HERMITIAN HAMILTONIAN OF COUPLED HARMONIC OSCILLATORS

In this section we map the CHO equations of motion to the two-state non-Hermitian Hamiltonian (NHH). The NHH we derive is similar to the Hamiltonian of a two state perturbed system (as discussed in introductory quantum mechanics textbooks[40]), with the important difference that for the NHH the energy spectrum is complex. As we will see, the imaginary part of the energy is directly related to the losses, i.e. the fact that

the oscillators are in contact with a reservoir (air) where they dissipate energy.

We start by inserting the ansatz $x_j(t) = x_j^0 e^{-i\omega t}$ in Eq. 1, and writing the equations in matrix form. Next, dividing the first row by $\omega_1 + \omega$ and the second row by $\omega_2 + \omega$, we get

$$\begin{bmatrix} \omega_1 - \omega - \frac{i\gamma_1\omega}{(\omega_1+\omega)} & -\frac{\Omega^2}{(\omega_1+\omega)} \\ -\frac{\Omega^2}{(\omega_2+\omega)} & \omega_2 - \omega - \frac{i\gamma_2\omega}{(\omega_2+\omega)} \end{bmatrix} \begin{bmatrix} x_1 \\ x_2 \end{bmatrix} = \begin{bmatrix} 0 \\ 0 \end{bmatrix}. \quad (8)$$

Since we are interested in the response of the system at or near resonance, we assume $|\omega - \omega_{1,2}| \ll \omega$. Under this approximation and defining $\bar{\omega} \approx (\omega + \omega_{1,2})/2$ as the mean frequency, Eq. 8 becomes

$$\begin{bmatrix} \omega_1 - \frac{i\gamma_1}{2} - \omega & -\frac{\Omega^2}{2\bar{\omega}} \\ -\frac{\Omega^2}{2\bar{\omega}} & \omega_2 - \frac{i\gamma_2}{2} - \omega \end{bmatrix} \begin{bmatrix} x_1 \\ x_2 \end{bmatrix} = \begin{bmatrix} 0 \\ 0 \end{bmatrix}. \quad (9)$$

Equation 9 has non-trivial solutions if the determinant of the left-most term vanishes. Hence, we need to solve the characteristic equation $|H - \omega I| = 0$, where I is the identity matrix and

$$H = \begin{bmatrix} \omega_1 - \frac{i\gamma_1}{2} & g \\ g & \omega_2 - \frac{i\gamma_2}{2} \end{bmatrix}, \quad (10)$$

with $g = -\frac{\Omega^2}{2\bar{\omega}}$ the effective coupling constant.

Equation 10 defines, in units of $\hbar = 1$, the two-state NHH corresponding to the CHOs. Through diagonalization and a little bit of algebra, we can write the eigenvalues of the NHH in the following form,

$$\omega_{\pm} = \tilde{\omega} \pm \frac{\Delta}{2}\sqrt{1 + \left(\frac{2g}{\Delta}\right)^2}, \quad (11)$$

where we have defined $\tilde{\omega} = (\omega_1 + \omega_2)/2 - i(\gamma_1 + \gamma_2)/4$ as the average complex frequency of the bare states, and $\Delta = (\omega_1 - \omega_2) - i(\gamma_1 - \gamma_2)/2$ as their complex detuning. Physically, the real and imaginary parts of $\omega_{\pm}$ are associated with the peak frequencies and linewidths of decay resonances, respectively. We will denote these as follows: $\omega_{\pm} = \omega_{\pm}' - i\omega_{\pm}''/2$. For the particular case of a lossless ($\gamma_1 = \gamma_2 = 0$) degenerate ($\omega_1 = \omega_2$) system, the eigenvalues (energies given our convention $\hbar = 1$) in Eq. 11 are those predicted by first-order time-independent degenerate perturbation theory[40]. They constitute the spectrum of a Hermitian Hamiltonian describing a conservative two-state quantum system under the influence of a perturbation with a strength proportional to g.

The mapping of the classical equations of motion of CHOs to a non-Hermitian Hamiltonian sheds light on a connection between the physics of first order perturbation theory and coupled oscillators. This quantum-classical correspondence suggests that allowing Hamiltonians to be non-Hermitian in quantum mechanics amounts to allowing oscillators to be damped in classical mechanics. While the latter is common practice at the

undergradaute level, the former is currently not. Since the non-Hermitian framework is becoming increasingly relevant at various fronts of physics,[29–34] the present discussion conveys a simple approach through which advanced undergraduates or graduate students can be introduced to this topic.

Let us now analyze several of the general properties of the complex eigenfrequencies $\omega_{\pm}$. We do this through analytical inspection of equation 11. Taylor expanding the square root term at $\frac{2g}{\Delta} = 0$ yields,

$$\omega_{\pm} \approx \tilde{\omega} \pm \frac{\Delta}{2}\left(1 + \left(\frac{2g}{\Delta}\right)^2 - \left(\frac{2g}{\Delta}\right)^4 \dots\right). \quad (12)$$

Retaining only the leading term yields the frequencies of the bare states, i.e. $\omega_{\pm} = \tilde{\omega} \pm \Delta/2$. It follows that the influence of the coupling constant g on $\omega_{\pm}$ is negligible, or weak, as $\Delta \to \infty$.

We also recognize from equation 11 that the square root term is singular at $2g/\Delta = \pm i$. The existence of this pole in the complex Δ plane implies that the perturbation series of $\omega_{\pm}$ in powers of $2g/\Delta$ converges inside a disk of radius $|2g/\Delta| = 1$. For $|2g/\Delta| \geq 1$, $\omega_{\pm}$ can not be analytically calculated by considering $2g/\Delta$ as a perturbation. This non-perturbative regime is therefore known as the strong coupling regime.

There are two important differences between the above definition of strong coupling and the one discussed in previous sections. Firstly, under the criterion derived in the present section, the ratio of the coupling constant to the individual loss rates or their sum imposes no restriction in defining the strong coupling regime. Secondly, the boundary between weak and strong coupling as determined by the perturbative or non-perturbative character of the parameter $|2g/\Delta|$ is sharp. This sharpness is determined by the existence of a pole in the complex plane. In previous sections, energy exchange cycles and/or frequency splitting appeared smoothly as the parameter $\Omega^2/\omega_0\gamma$ increased above unity.

Next we illustrate the general behavior of $\omega_{\pm}$ in the complex Δ plane. For brevity, we define $\Delta' = \omega_1 - \omega_2$ and $\Delta'' = (\gamma_1 - \gamma_2)/2$ as the real and imaginary parts of the complex detuning $\Delta = \Delta' - i\Delta''$. The real part of $\omega_{\pm}$ is plotted in Fig.8(a), and the imaginary part of $\omega_{\pm}$ is plotted in Fig. 8(b). All quantities in Fig. 6 are divided by $2g$ to render all axes dimensionless.

Figure 6 shows $\omega_{\pm}'$ and $\omega_{\pm}''$ in the complex plane. Interestingly, at $\Delta''/2g = \pm 1$ and $\Delta' = 0$ both the real and imaginary parts of ω_+ and ω_- coalesce. This is the so-called exceptional point (EP) at the heart of Non-Hermitian quantum mechanics.[29] The EP defines the boundary between strong and weak coupling. In contrast with a 2×2 Hermitian Hamiltonian involving purely real detuning ($\Delta'' = 0$), Fig. 6 shows that the eigenvalues of the NHH are analytic continuations of each other via the EP. Thus, by continuously varying Δ one energy level of the system is transformed into another.
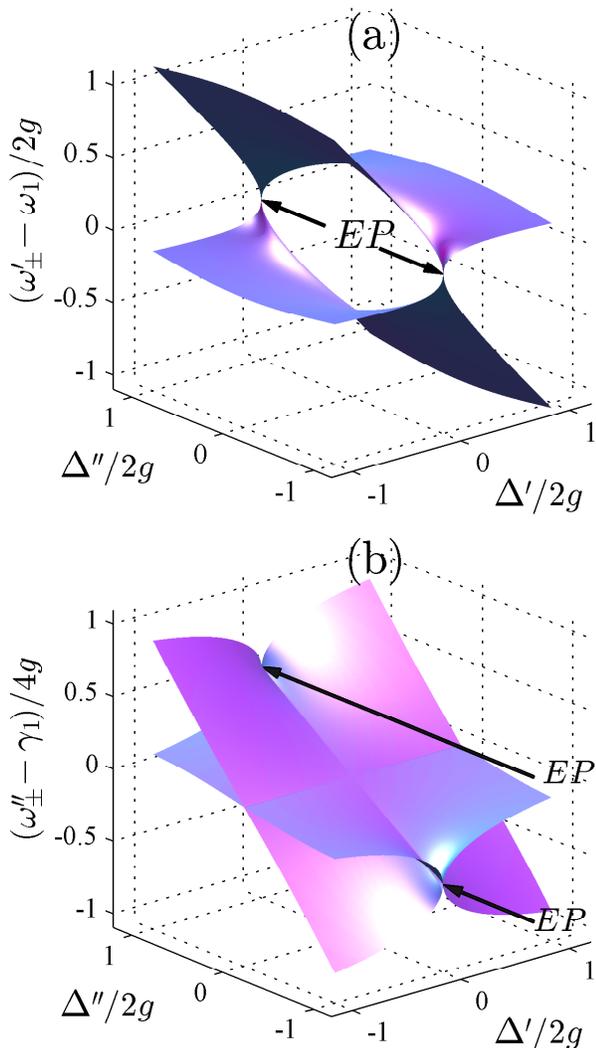
FIG. 6. (a) Real and (b) Imaginary parts of the non-Hermitian Hamiltonian eigenvalues plotted in the complex detuning plane. $\Delta' = \omega_1 - \omega_2$ is the real detuning and $\Delta'' = (\gamma_1 - \gamma_2)/2$ is the imaginary detuning. All quantities are divided by $2g$, with g the coupling constant, such that all axes are dimensionless. The exceptional points (EP) are indicated by the arrows.

To visualize the EP and its vicinity more clearly, we plot in Fig. 7(a) and Fig. 7(b) cuts of Fig. 6(a) and Fig. 6(b), respectively. In both panels we plot $\omega_\pm$ as a function $\Delta'/2g$ for three different values of $\Delta''/2g$. The blue dashed lines correspond to $\Delta''/2g = 0.9$, the black solid lines correspond to $\Delta''/2g = 1$, and the red dash-dotted lines correspond to $\Delta''/2g = 1.1$. The blue dashed and red dash-dotted lines illustrate the general structure of the NHH spectrum: level crossings imply anti-crossings of the corresponding resonance linewidths and viceversa.[41] However, at the EP both real and imaginary parts cross (black solid lines). There are various other fascinating aspects of the EP; we refer to Moiseyev for further details.[29]
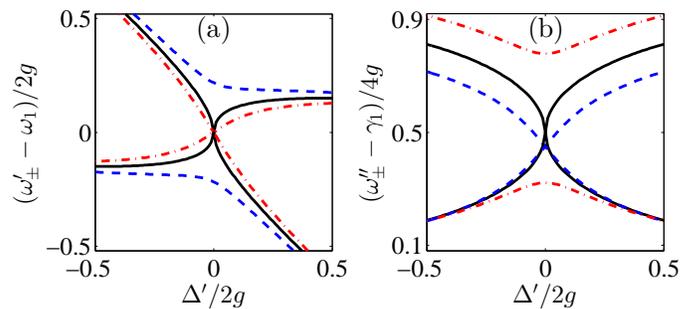

FIG. 7. (a) and (b) are cuts of Fig. 6(a) and Fig. 6(b), respectively, at different values of $\Delta''/2g$. $\Delta''/2g = 1$ for the black solid lines , $\Delta''/2g = 0.9$ for the blue dashed lines, and $\Delta''/2g = 1.1$ for the red dash-dotted lines. The exceptional point is at $\Delta''/2g = 1$ and $\Delta'/2g = 0$, where both real and imaginary parts of $\omega_\pm$ cross.

V. CONCLUDING REMARKS

In section II we discussed the existence of two dynamical regimes based on the presence or absence of at least one cycle of energy exchange between CHOs. A single cycle of energy exchange corresponds to an observable resonance frequency splitting in the time-integrated power spectrum. Similarly, in section III we showed that the steady-state response of a driven CHO system displays an identical frequency splitting and an avoided resonance crossing under the same condition: $\Omega^2/\omega_0\gamma \gtrsim 1$. For both the dynamics and the steady-state response, the transition from weak to strong coupling as $\Omega^2/\omega_0\gamma$ increases above unity is smooth.

In section IV we mapped the CHO equations of motion to the two-state non-Hermitian Hamiltonian (NHH). Therein, we found that strong coupling corresponds to $|2g/\Delta| \geq 1$, with g the coupling constant and Δ the complex detuning between the bare states. This condition is based on the analytic properties of the NHH eigenvalues (energies) as a series in powers of $2g/\Delta$. In particular, weak and strong coupling are the regimes for which $2g/\Delta$ is perturbative or not, respectively. The distinction in this case is sharp; it is based on the presence of a pole in the complex plane.

The two criteria for strong coupling we discussed ($\Omega^2/\omega_0\gamma \gtrsim 1$ and $2g/\Delta \geq 1$) give the same result for many systems deep in the strong or weak coupling regimes. However, we have seen that certain systems can comply with one criterion but not the other. Firstly, in Fig. 2(a) we presented a system for which $\Omega^2/\omega_0\gamma < 1$ and $|2g/\Delta| \gg 1$, thereby complying with the second condition for strong coupling without displaying energy exchange cycles. Next, in Fig. 3(a) and Fig. 3(b) we considered systems with unequal eigenfrequencies and loss rates, respectively. The former sustained multiple (incomplete) energy exchange cycles, while the latter showed a single cycle of energy exchange. Therefore, while both systems in Fig. 3 display energy exchange cy-

cles, the condition $|2g/\Delta| \geq 1$ is not fulfilled. In view of these results, it is clear that the two definitions of strong coupling can not in general be used interchangeably. An anti-crossing of real eigenvalues does not imply energy exchange cycles or avoided resonance crossings and viceversa.

Understanding the physical differences associated with the distinct criteria for strong coupling is especially critical in studies of energy transfer. For example, the authors of Ref. 26 plotted calculated eigenvalues on top of measured reflectivity data in order to quantify energy transfer between molecules and a metallic structure. Interestingly, for some data sets the eigenvalues anti-cross while the measurements display single, at most weakly perturbed, resonance. Energy transfer is largely overwhelmed by dissipation in such cases (no energy exchange cycles). Another interesting example of how the model and approach employed can lead to significantly different conclusions transpires from comparing Ref. 25 with Ref. 42. In Ref. 25 the authors observe a modest, but well-visible, avoided resonance crossing, and they conclude that they only approach but not fully reach the strong coupling regime. In contrast, in Ref. 42 a smaller frequency splitting, which is well below the largest resonance linewidth, is observed. Nevertheless, the authors claim to observe the strong coupling regime based on the anti-crossing of the real part of the resonance energy (eigenvalue)[42]. These two different interpretations, here taken as an example, are likely due to the use of different models and approaches. These examples illustrate why it is relevant to look at each system in different ways, and to raise awareness about the physical effects defining the boundary between weak and strong coupling in different formalisms.

Finally, it is worth mentioning that while a classical analog to strong coupling based on CHOs was presented in Ref. 3, the analogy relied on the anti-crossing of the eigenvalues of a lossless system. However, lossless systems can not in general define a boundary between weak and strong coupling. Every lossless system tuned in resonance is "strongly coupled" for any nonzero energy exchange rate. It is only through the inclusion of losses and the departure from the Hermitian framework that the different features of weak and strong coupling in the classical and quantum descriptions can be recognized. Students can be introduced to all of these features, and to the key ideas of the non-Hermitian quantum framework, through mechanical models of CHOs or through their electrical counterparts which have proven successful in undergraduate laboratories worldwide [7,14,16].

* said.rodriguez@lpn.cnrs.fr
† current address:Laboratoire de Photonique et de Nanostructures, LPN/CNRS, Route de Nozay, 91460 Marcoussis, France
[1] A. J. Leggett, S. Chakravarty, A. T. Dorsey, Matthew P. A. Fisher, Anupam Garg, and W. Zwerger, "Dynamics of the dissipative two-state system," Rev. Mod. Phys. 59, 1–85 (1987).
[2] D. Dragoman and M. Dragoman, Quantum-Classical Analogies, The Frontiers Collection (Springer, 2014).
[3] Lukas Novotny, "Strong coupling, energy splitting, and level crossings: A classical perspective," Am. J. Phys. 78, 1199–1202 (2010).
[4] P Törmä and W L Barnes, "Strong coupling between surface plasmon polaritons and emitters: a review," Rep. Prog. Phys. 78, 013901 (2015).
[5] Lucio Claudio Andreani, "Exciton-polaritons in bulk semiconductors and in confined electron and photon systems," in Strong Light-Matter Coupling, Chap. 2, pp. 37–82.
[6] Fabrice P. Laussy, Elena del Valle, and Carlos Tejedor, "Luminescence spectra of quantum dots in microcavities. i. Bosons," Phys. Rev. B 79, 235325 (2009).
[7] C. L. Garrido Alzar, M. A. G. Martinez, and P. Nussenzveig, "Classical analog of electromagnetically induced transparency," Am. J. Phys. 70, 37–41 (2002).
[8] Yong S Joe, Arkady M Satanin, and Chang Sub Kim, "Classical analogy of Fano resonances," Phys. Scripta 74, 259 (2006).
[9] B. W. Shore, M. V. Gromovyy, L. P. Yatsenko, and V. I. Romanenko, "Simple mechanical analogs of rapid adiabatic passage in atomic physics," Am. J. Phys. 77 (2009).
[10] Na Liu, Lutz Langguth, Thomas Weiss, Jürgen Kästel, Michael Fleischhauer, Tilman Pfau, and Harald Giessen, "Plasmonic analogue of electromagnetically induced transparency at the Drude damping limit," Nature Mater. 8, 758–762 (2009).
[11] Shaunak Mukherjee, Heidar Sobhani, J. Britt Lassiter, Rizia Bardhan, Peter Nordlander, and Naomi J. Halas, "Fanoshells: Nanoparticles with Built-in Fano Resonances," Nano Lett. 10, 2694–2701 (2010).
[12] Andrey E. Miroshnichenko, Sergej Flach, and Yuri S. Kivshar, "Fano resonances in nanoscale structures," Rev. Mod. Phys. 82, 2257–2298 (2010).
[13] Bruce W Shore, Manipulating quantum structures using laser pulses (Cambridge University Press, 2011).
[14] Joshua Harden, Amitabh Joshi, and Juan D Serna, "Demonstration of double EIT using coupled harmonic oscillators and RLC circuits," Eur. J. Phys. 32, 541 (2011).

[15] Philippe Tassin, Lei Zhang, Rongkuo Zhao, Aditya Jain, Thomas Koschny, and Costas M. Soukoulis, "Electromagnetically induced transparency and absorption in metamaterials: The radiating two-oscillator model and its experimental confirmation," Phys. Rev. Lett. **109**, 187401 (2012).

[16] S. Satpathy, A. Roy, and A. Mohapatra, "Fano interference in classical oscillators," Eur. J. Phys. **33**, 863 (2012).

[17] John S. Briggs and Alexander Eisfeld, "Equivalence of quantum and classical coherence in electronic energy transfer," Phys. Rev. E **83**, 051911 (2011).

[18] John S. Briggs and Alexander Eisfeld, "Coherent quantum states from classical oscillator amplitudes," Phys. Rev. A **85**, 052111 (2012).

[19] John S. Briggs and Alexander Eisfeld, "Quantum dynamics simulation with classical oscillators," Phys. Rev. A **88**, 062104 (2013).

[20] Carl M. Bender, Mariagiovanna Gianfreda, Şahin K. Özdemir, Bo Peng, and Lan Yang, "Twofold transition in $\mathcal{PT}$-symmetric coupled oscillators," Phys. Rev. A **88**, 062111 (2013).

[21] Martin Frimmer and Lukas Novotny, "The classical Bloch equations," Am. J. Phys. **82**, 947–954 (2014).

[22] D. G. Lidzey, D. D. C. Bradley, M. S. Skolnick, T. Virgili, S. Walker, and D. M. Whittaker, "Strong exciton-photon coupling in an organic semiconductor microcavity," Nature **395**, 53–55 (1998).

[23] Simon Groblacher, Klemens Hammerer, Michael R. Vanner, and Markus Aspelmeyer, "Observation of strong coupling between a micromechanical resonator and an optical cavity field," Nature **460**, 724–727 (2009).

[24] E. Verhagen, S. Deleglise, S. Weis, A. Schliesser, and T. J. Kippenberg, "Quantum-coherent coupling of a mechanical oscillator to an optical cavity mode," Nature **482**, 63–67 (2012).

[25] G. Zengin, G. Johansson, P. Johansson, T.J. Antosiewicz, M. Käll, and T. Shegai, "Approaching the strong coupling limit in single plasmonic nanorods interacting with j-aggregates," Sci. Rep. **3**, 3074 (2013).

[26] Mikko A. Koponen, Ulrich Hohenester, Tommi K. Hakala, and J. Jussi Toppari, "Absence of mutual polariton scattering for strongly coupled surface plasmon polaritons and dye molecules with a large stokes shift," Phys. Rev. B **88**, 085425 (2013).

[27] S. R. K. Rodriguez, Y. T. Chen, T. P. Steinbusch, M. A. Verschuuren, A. F. Koenderink, and J. Gómez Rivas, "From weak to strong coupling of localized surface plasmons to guided modes in a luminescent slab," Phys. Rev. B **90**, 235406 (2014).

[28] Xiaoze Liu, Tal Galfsky, Zheng Sun, Fengnian Xia, Erhchen Lin, Yi-Hsien Lee, Stéphane Kéna-Cohen, and Vinod M. Menon, "Strong light–matter coupling in two-dimensional atomic crystals," Nature Photon. **9**, 30–34 (2015).

[29] Nimrod Moiseyev, *Non-Hermitian quantum mechanics* (Cambridge University Press, 2011).

[30] M. Philipp, P. von Brentano, G. Pascovici, and A. Richter, "Frequency and width crossing of two interacting resonances in a microwave cavity," Phys. Rev. E **62**, 1922–1926 (2000).

[31] C. Dembowski, H.-D. Gräf, H. L. Harney, A. Heine, W. D. Heiss, H. Rehfeld, and A. Richter, "Experimental observation of the topological structure of exceptional points," Phys. Rev. Lett. **86**, 787–790 (2001).

[32] W D Heiss, "The physics of exceptional points," J. Phys. A Math. Theor. **45**, 444016 (2012).

[33] Christian E Rüter, Konstantinos G Makris, Ramy El-Ganainy, Demetrios N Christodoulides, Mordechai Segev, and Detlef Kip, "Observation of parity–time symmetry in optics," Nature Phys. **6**, 192–195 (2010).

[34] Bo Peng, Şahin Kaya Özdemir, Fuchuan Lei, Faraz Monifi, Mariagiovanna Gianfreda, Gui Lu Long, Shanhui Fan, Franco Nori, Carl M Bender, and Lan Yang, "Parity-time-symmetric whispering-gallery microcavities," Nature Phys. **10**, 394–398 (2014).

[35] B. W. Shore and N. V. Vitanov, "Overdamping of coherently driven quantum systems," Contemp. Phys. **47**, 341–362 (2006).

[36] G. S. Agarwal, "Vacuum-field Rabi oscillations of atoms in a cavity," J. Opt. Soc. Am. B **2**, 480–485 (1985).

[37] S. R. K. Rodriguez, S. Murai, M. A. Verschuuren, and J. Gómez Rivas, "Light-Emitting Waveguide-Plasmon Polaritons," Phys. Rev. Lett. **109**, 166803 (2012).

[38] V. Savona, L.C. Andreani, P. Schwendimann, and A. Quattropani, "Quantum well excitons in semiconductor microcavities: Unified treatment of weak and strong coupling regimes," Solid State Commun. **93**, 733 – 739 (1995).

[39] T. Schwartz, J. A. Hutchison, C. Genet, and T. W. Ebbesen, "Reversible switching of ultrastrong light-molecule coupling," Phys. Rev. Lett. **106**, 196405 (2011).

[40] D.J. Griffiths, *Introduction to Quantum Mechanics*, Pearson international edition (Pearson Prentice Hall, 2005).

[41] W. D. Heiss, "Repulsion of resonance states and exceptional points," Phys. Rev. E **61**, 929–932 (2000).

[42] Anne-Laure Baudrion, Antoine Perron, Alessandro Veltri, Alexandre Bouhelier, Pierre-Michel Adam, and Renaud Bachelot, "Reversible strong coupling in silver nanoparticle arrays using photochromic molecules," Nano Lett. **13**, 282–286 (2013).